

# Commensurate and Incommensurate Ordering Tendencies in the Ternary fcc Cu-Ni-Zn System

J. D. Althoff,<sup>1</sup> D. D. Johnson,<sup>1</sup> and F. J. Pinski<sup>2</sup>

<sup>1</sup>Computational Materials Science Department, Sandia National Laboratories, MS 9161, Livermore, California 94551

<sup>2</sup>Department of Physics, University of Cincinnati, Cincinnati, Ohio 45221-0011

(Received 1 June 1994)

We show that Fermi-surface (FS) nesting drives both the incommensurate *and* commensurate ordering tendencies of the fcc ternary Cu-Ni-Zn system. Surprisingly, commensurate order persists over a wide range of composition, despite its origins. For Cu<sub>2</sub>NiZn, we discuss how FS nesting and the other effects of alloying lead to ordering tendencies consistent with the experimentally observed order-disorder transformations. All calculations are based on a first-principles theory of the atomic short-range order in alloys with an *arbitrary* number of components.

PACS numbers: 71.20.Cf, 64.60.Cn, 75.40.Cx

While there has been much work on long- and short-range order in binary alloys [1–3], very little theoretical insight has been developed for ternary (or, more generally, *N*-component) systems [3]. As a step toward understanding the basic driving forces in such systems, we have developed a first-principles theory of atomic short-range order (ASRO) in alloys of an *arbitrary* number of components [4] and here apply it to the Cu-Ni-Zn system. The fcc ternary system Cu-Ni-Zn is especially interesting because it exhibits a wide range of ordering tendencies: both incommensurate and commensurate chemical ordering and phase separation [5–8]. We show that the chemical ordering, both incommensurate *and* commensurate, is driven by Fermi-surface (FS) nesting effects, contrary to what has been assumed by previous authors [9–11]. Surprisingly, commensurate order persists over a wide concentration range, as observed [6], despite its FS origin. We first focus on the ASRO and order-disorder transformations in the experimentally well-characterized alloy Cu<sub>2</sub>NiZn and then discuss how changes in the alloy composition affect the ASRO through their influence on the FS properties. Note that since we are working with ternary alloys the composition and electron per atom ratio (*e/a*) can be varied independently.

It is known experimentally that a variety of commensurate and incommensurate ASRO exists in the Cu-Ni-Zn system. Van der Wegen *et al.* [8,12] observed that Cu<sub>2</sub>NiZn undergoes two first-order phase transitions. The first, at about 774 K, is from a (disordered) fcc solid solution to a partially ordered modified *L1*<sub>2</sub> structure in which the Zn atoms preferentially occupy the corners of the fcc cube, with the face centers randomly occupied by Ni and Cu. In the second transition, at about 598 K, the occupations of the face centers order to a fully ordered modified *L1*<sub>0</sub> (modified Heusler) structure. Hashimoto *et al.* [9] performed diffuse x-ray scattering experiments on a Cu<sub>47</sub>Ni<sub>29</sub>Zn<sub>24</sub> sample quenched from 875 K to determine the ASRO and find ⟨100⟩-type ASRO. They dismissed the possibility of the FS being the origin. Experimentally [6], long-range order of ⟨100⟩-type occurs around the line

in the Gibbs triangle that connects the binary NiZn with pure Cu. Along this line, all alloys are isoelectronic with Cu, with Cu<sub>2</sub>NiZn sitting on this line. Moving off this line, Reinhard *et al.* [7] have measured incommensurate ASRO indicative of DO<sub>23</sub>-type order in Cu-rich fcc binary CuZn. On the other side, CuNi is a clustering alloy, showing  $\vec{k} = 0$  ASRO [5,13].

Our first-principles theory of ASRO for a multicomponent alloy is a mean-field theory of concentration fluctuations [1,14], and uses the multiple-scattering electronic-structure method of Korringa, Kohn, and Rostoker (KKR) combined with the coherent potential approximation (CPA) and (local) density functional theory to evaluate the electronic grand potential of the random state. A version of the theory for binary alloys has only recently been discussed [15,16] and some review and results for several binaries are presented in Refs. [2,15,16]. Because the theory is based directly on properties of the alloy electronic structure, it is possible to pinpoint the microscopic origins of the observed ordering tendencies in order to develop insight into the role of various, sometimes competing, effects, e.g., electronic structure, atomic size, and charge transfer.

Any alloy configuration can be specified by a set of occupation variables  $\{\xi_i^\alpha\}$ , where  $\xi_i^\alpha$  is 1 (0) if an  $\alpha$  species atom does (does not) occupy site *i*. The thermodynamic average  $\langle \xi_i^\alpha \rangle = c_i^\alpha$  is the concentration of species  $\alpha$  at site *i*. The  $\{\xi_i^\alpha\}$  are not all independent—we implement the single-occupancy constraint by designating the *N*th atomic species as the “host” and considering the host occupation  $\xi_i^N$  as a dependent variable. The ASRO is described by the atomic pair correlation function (a matrix in the species and site indices), defined as  $q_{ij}^{\mu\nu} = \langle \xi_i^\mu \xi_j^\nu \rangle - \langle \xi_i^\mu \rangle \langle \xi_j^\nu \rangle$ , which is related to the familiar Warren-Cowley short-range order parameter

$$\alpha_{\beta\gamma}(\vec{k}) = \frac{q_{\beta\gamma}(\vec{k})}{c_\beta(\delta_{\beta\gamma} - c_\gamma)} \quad (1)$$

derived from experiment. The theory yields directly a nonsingular portion of the inverse of the lattice Fourier-

transformed correlation function matrix,  $q^{\mu\nu}(\vec{k})$ , i.e., [4]

$$[q^{-1}(\vec{k}; T)]_{\mu\nu} = \left[ \delta_{\mu\nu} \frac{1}{c_\mu} + \frac{1}{c_N} \right] - \beta [S_{\mu\nu}^{(2)}(\vec{k}; T) - \Sigma_{\mu\nu}(T)], \quad (2)$$

where  $\beta = 1/k_B T$  and  $T$  is the absolute temperature. The central quantity of the theory is  $S_{\mu\nu}^{(2)}$ , which embodies all properties of the electronic structure, including electron-hole effects. Explicitly,  $S_{\mu\nu}^{(2)}(\vec{k})$  is the Fourier transform of

$$S_{ij}^{\mu\nu} = - \left( \frac{\partial^2 \langle \Omega_e \rangle_0}{\partial c_i^\mu \partial c_j^\nu} \right)_{c_i^\mu = \bar{c}^\mu \nabla_i; c_j^\nu = \bar{c}^\nu \nabla_j}, \quad (3)$$

where  $\langle \Omega_e \rangle_0$  is the electronic grand potential averaged with respect to a single-site probability distribution, as in [2,4,15,16], and is calculated within the KKR-CPA formalism. In the present work, we keep only the “band-energy” contributions to the second derivative, and defer a full treatment of the “double-counting” and displacive contributions to a later work. The quantity  $\Sigma_{\mu\nu}$  is the Onsager cavity-field correction to the mean-field theory, which ensures that the spectral intensity is conserved over the Brillouin zone, atypical of mean-field theories, and is discussed in Refs. [15,16]. The coupled integral equations that determine both  $S_{\mu\nu}^{(2)}(\vec{k})$  and  $q_{\mu\nu}$  are more general than those of the binary-only case—but, it turns out, no more difficult to implement—further details will be discussed in a forthcoming publication [4].

At the wave vector  $\vec{k}_0$  and spinodal temperature  $T_{sp}$ , the determinant of the inverse of the correlation function matrix [Eq. (2)] vanishes, signifying that the high-temperature, homogeneously disordered state is unstable to the formation of a concentration wave with wave vector  $\vec{k}_0$ . Although most order-disorder transformations in alloys are (experimentally) first-order transitions, the ASRO observed at high temperature is frequently a precursor of the low-temperature long-range order. In practice,  $T_{sp}$  is often close to the experimentally observed transition temperature [14–16]. The eigenvector of  $S_{\mu\nu}^{(2)}(\vec{k}_0, T_{sp})$  corresponding to the vanishing eigenvalue of  $q^{-1}$  describes the polarization of the concentration wave in composition space [4,17]. From the polarization and the wave vector  $\vec{k}_0$ , the atomic distribution may be determined [4,17].

In Fig. 1(a), we show the off-diagonal components of the Warren-Cowley matrix for  $\text{Cu}_2\text{NiZn}$  along the lines  $W$  to  $X$  to  $\Gamma$  in the fcc Brillouin zone at a temperature approximately 10% above  $T_{sp}$ . The squares correspond to our calculated points, and the lines are obtained by first finding a least-squares real-space (lattice Fourier series) fit to the calculated  $S_{\mu\nu}^{(2)}(\vec{k})$  and then calculating the corresponding  $\alpha_{\beta\gamma}(\vec{k})$ . The real-space fit, in principle, yields real-space interaction parameters, which are sometimes useful in interpreting the results. For  $\text{Cu}_2\text{NiZn}$ , we are able to achieve an exceptional fit with 35 nearest-neighbor shells. The Ni-Zn correlation

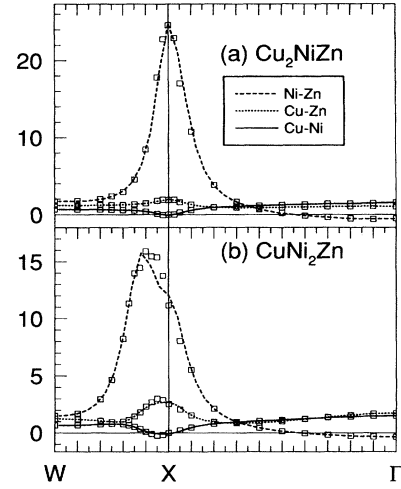


FIG. 1. The Ni-Zn (---), Cu-Zn (···), and CuNi (—) Warren-Cowley SRO parameters in Laue units for (a)  $\text{Cu}_2\text{NiZn}$  and (b)  $\text{CuNi}_2\text{Zn}$ . The squares (lines) are the calculated points in  $\vec{k}$  space (the real-space fit, see text).

is clearly the strongest and is sharply peaked at  $\vec{k} = \langle 100 \rangle$ . The much weaker Cu-Zn interaction also favors  $\langle 100 \rangle$  ASRO. Since binary Cu-Ni clusters [5,13], it is interesting that the Cu-Ni correlation is almost zero at the  $X$  point, goes negative as the temperature is lowered further, and has a maximum at  $\vec{k} = (000)$ , indicative of the clustering tendency. Because of this very strong Ni-Zn correlation, we expect that the system will undergo a transition to a state with  $\langle 100 \rangle$  long-range order in which the Ni and Zn atoms occupy different sublattices.

The off-diagonal Ni-Zn component of the calculated correlation function matrix for  $\text{Cu}_2\text{NiZn}$  diverges at  $\vec{k}_0 = \langle 100 \rangle$  and  $T_{sp} = 980$  K (1240 K without Onsager corrections). The corresponding eigenvector of  $S^{(2)}$  describes a structure composed of four interpenetrating simple cubic lattices, where on one sublattice the probability for finding Zn is greatly enhanced and the probability for finding Cu or Ni is correspondingly reduced; on the remaining three sublattices the situation is reversed. This is consistent with the partially ordered modified  $L1_2$  structure seen experimentally [8,12]. Further, given  $\vec{k}_0$  and the alloy composition, the theory of concentration waves [14] constructs, on the basis of symmetry alone, the fully ordered modified  $L1_0$  structure seen experimentally [4]. Since this partially ordered state has a different atomic distribution than the fully ordered state, a second transition to the fully ordered state will take place, provided there are no interloper phases. Because of the strength of the Ni-Zn correlation, it is unlikely that any such interloper phases exist.

While our results agree qualitatively with the experimental results of Hashimoto *et al.* [9], a detailed quantitative comparison is impossible for two reasons. First, the experimental data strongly violate the sum rules gov-

erning the integrated diffuse intensities over the Brillouin zone, as noted by Hashimoto *et al.* [9]. Within our calculations, these sum rules are enforced via the Onsager reaction field  $\Sigma_{\mu\nu}$ . Second, the values of the partial diffuse intensities found in the experiment are an order of magnitude larger than what is typically seen that far above  $T_c$ , and are indicative of ASRO at a temperature much closer to  $T_c$  than the temperature from which the sample was quenched. Of course, if in our calculation we lower the temperature closer to the spinodal, we too find very large values of the ASRO at  $\langle 100 \rangle$ .

When the ASRO arises mainly from electronic structure near the Fermi level, it is instructive to write  $S_{\mu\nu}^{(2)}$  approximately as [2,18]

$$S_{\mu\nu}^{(2)}(\vec{q}) \sim \int d\epsilon \int d\epsilon' M_{\mu\nu}(\epsilon) \frac{f(\epsilon) - f(\epsilon')}{\epsilon - \epsilon'} \times \int d\vec{k} A(\vec{k}; \epsilon') A(\vec{k} + \vec{q}; \epsilon), \quad (4)$$

where  $M_{\mu\nu}(\epsilon)$  is a species- and energy-dependent matrix element and  $A(\vec{k}; \epsilon)$  is the Bloch spectral function (BSF) [2]; in such a picture  $S_{\mu\nu}^{(2)}$  has the appearance of a generalized susceptibility. The presence of the Fermi factors and energy denominators in (4) can lead to a large contribution from energies near the Fermi level;  $A(\vec{k}; \epsilon_F)$  describes the “Fermi surface” of the random alloy. Thus, if the FS and its image shifted in reciprocal space by the wave vector  $\vec{Q}$  have a large overlap, a large value of  $S_{\mu\nu}^{(2)}$  at that wave vector (and all symmetry related wave vectors) will result. Within this framework, this is a mathematical statement of the FS nesting ideas discussed by Moss [19]. In general,  $\vec{Q}$  is not a high symmetry wave vector and is incommensurate with the lattice periodicity—this leads to the familiar fourfold splitting of diffuse scattering peaks as seen, for example, in  $\text{Cu}_3\text{Zn}$  [4,7]. In contrast, if  $\vec{Q}$  is a high symmetry point, FS nesting leads to commensurate order. One would expect that this would be most unusual, but it is indeed what we find for  $\text{Cu}_2\text{NiZn}$  and other alloys isoelectronic with it.

In Fig. 2, we plot the BSF at the Fermi energy (the alloy FS) for disordered  $\text{Cu}_2\text{NiZn}$  in the  $k_z = 0$  plane. The FS is very boxlike and is broadened by disorder. This disorder broadening actually serves to increase the overlap between  $A(\vec{k}; \epsilon_F)$  and  $A(\vec{k} + \vec{k}_0; \epsilon_F)$ , leading to a large value of the convolution integral (4) for  $\vec{k}_0 = \langle 100 \rangle$ . The flat portions of the FS in the  $k_z = 0$  plane evident in Fig. 2 extend out of the plane for some distance. Alloying changes the familiar “dog-bone” structure of the pure Cu FS [20] into a “bow tie” structure with flatter edges, further enhancing the nesting. This particular feature improves the nesting for the incommensurate cases, e.g.,  $\text{CuNi}_2\text{Zn}$ . The Fermi level lies in the  $s$ - $p$  bands for this alloy, and it is the common  $s$ - $p$  band that plays a large role in establishing the ASRO.

As the alloy composition changes, two important features of the FS change. In some crude sense, when the Fermi level lies in the  $s$ - $p$  band, the dimensions of the

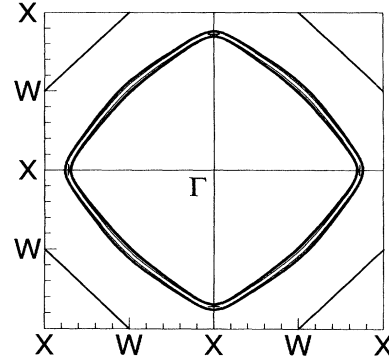


FIG. 2. Contour plot of the Bloch spectral function in the first Brillouin zone for  $\text{Cu}_2\text{NiZn}$  at the Fermi energy, i.e., the alloy Fermi surface, in the  $k_z = 0$  plane.

FS (e.g., the nesting vector, if there is one) depend primarily on  $e/a$ . Indeed, as the alloy composition is varied along the line in the Gibbs triangle for which  $e/a$  is constant and equal to that of pure Cu, we find that the magnitude of the nesting vector is approximately constant and that FS nesting leads to  $\langle 100 \rangle$ -type ASRO. The shape and sharpness of the FS do change, which affects the extent of the nesting and changes  $T_{sp}$ . This is illustrated in Fig. 3, where we show our results for several alloys of the Cu-Ni-Zn system. In agreement with experiment [6], we find a broad region of  $\langle 100 \rangle$  ASRO along the line  $\text{Cu}_x(\text{NiZn})_{1-x}$  (the Cu-isoelectronic line), as evidenced by our results for  $\text{Cu}_2\text{NiZn}$ ,  $\text{CuNiZn}$ , and  $\text{NiZn}$ . The extent of the region of  $\langle 100 \rangle$  ASRO is roughly indicated by our results for  $\text{Cu}_3\text{Ni}_3\text{Zn}_2$  and  $\text{CuNiZn}_2$ , which both show  $\langle 100 \rangle$  ASRO. Calculations for binary  $\text{NiZn}$  [4] also show  $\langle 100 \rangle$  ASRO, consistent with the observed [5]  $L1_0$  ground state, although there is experimentally [5] an entropy-driven ordered  $B2$  phase at high temperatures.

As one moves off of the Cu-isoelectronic line, changing  $e/a$ , the volume enclosed by the FS changes and so the magnitude of the nesting vector must ultimately change, leading to incommensurate ASRO. As we move away from  $\text{Cu}_2\text{NiZn}$  along the line  $\text{Cu}_{3-x}\text{Ni}_x\text{Zn}$ , we find in-

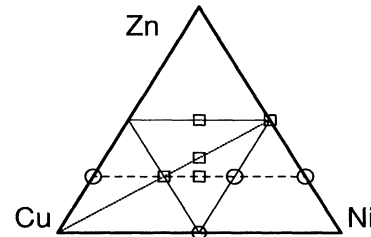


FIG. 3. Gibbs triangle of the Cu-Ni-Zn system in atomic percent. The dotted line is the Cu-isoelectronic line. The ASRO we find is as follows: squares,  $\langle 100 \rangle$  ASRO; circles, incommensurate ASRO; hexagon,  $\vec{k} = (000)$  ASRO.

commensurate ASRO for  $\text{Cu}_3\text{Zn}$  (as seen experimentally by Rheinhard *et al.* [7]) and for  $\text{CuNi}_2\text{Zn}$ , as shown in Fig. 3. This gives some idea of where the boundary of the region of  $\langle 100 \rangle$  ASRO lies, and is in good agreement with experiment [6]. In the Zn-poor region, we find clustering tendencies for binary CuNi [4], in agreement with experiment [5,13]. Experimentally, in the Zn-rich region of the phase diagram, there are found both bcc and hcp phases; we are currently investigating different crystal structures, and we are interested here only in the fcc phases.

To illustrate the effect of decreasing  $e/a$ , in Fig. 4 we show the FS for  $\text{CuNi}_2\text{Zn}$ . The FS is strongly nested (i.e., boxlike), and broader than that of  $\text{Cu}_2\text{NiZn}$ . In this case the volume enclosed by the FS has decreased and the ASRO has become incommensurate, with a dominant wave vector of approximately  $(0, 0.1, 1)$  and a  $T_{\text{sp}}$  of 485 K. In Fig. 1(b), we display the off-diagonal components of the Warren-Cowley matrix for  $\text{CuNi}_2\text{Zn}$  along the lines  $W$  to  $X$  and  $X$  to  $\Gamma$  in the fcc Brillouin zone, again calculated at 10% above  $T_{\text{sp}}$ . The Ni-Zn correlation is once again the strongest, but peaks at  $\vec{k} = (0, 0.1, 1.0)$ . As for  $\text{Cu}_2\text{NiZn}$ , the squares are the actual calculated data and the lines are  $\alpha_{\beta\gamma}(\vec{k})$  obtained from the real-space fit to  $S_{\mu\nu}^{(2)}(\vec{k})$ . For  $\text{CuNi}_2\text{Zn}$  the quality of the fit is much poorer (even with the 50 shells used here) than for  $\text{Cu}_2\text{NiZn}$ . The FS origin of these interactions, especially in the case of incommensurate ASRO, requires extremely long-ranged real-space interactions in order to reproduce the correlation function. As a result, while it is possible to reproduce the observed long-range order for  $\text{Cu}_2\text{NiZn}$  with only two nearest-neighbor interactions [3,10] or short-range cluster interactions [11], such a model will not describe the ternary system in general.

In conclusion, we have implemented a first-principles mean-field theory of ASRO in alloys of an arbitrary number of components, and applied it to several fcc Cu-Ni-Zn alloys. We have determined that the *commensurate*

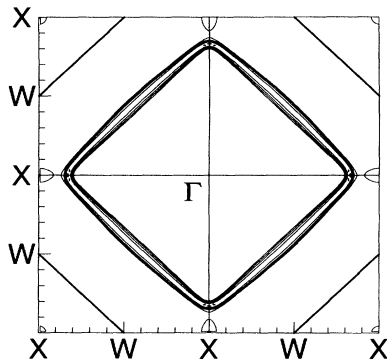


FIG. 4. As in Fig. 2, but for  $\text{CuNi}_2\text{Zn}$ .

$\vec{k} = \langle 1, 0, 0 \rangle$  ASRO arises due to FS effects and persists over a region surrounding the Cu-isoelectronic line, in agreement with experiment [6]. Elsewhere we find incommensurate ASRO, as expected from FS dimensions. For  $\text{Cu}_2\text{NiZn}$ , we find ASRO in the disordered solid solution that is consistent with the partially ordered phase at high temperatures, and, because of the strength of the Ni-Zn interaction, symmetry arguments alone require that the modified  $L1_0$  structure is stable at low temperatures.

This work was supported by the U.S. Department of Energy, Office of Basic Energy Sciences, Division of Materials Science through a New Initiative, under Contract No. DE-AC04-94AL85000, and by the National Science Foundation Grant No. DMR 9217297. We thank G.S. Bales and M.D. Asta for critical readings of the manuscript and J. B. Staunton for helpful discussions.

- [1] D. de Fontaine, *Solid State Phys.* **34**, 73 (1979).
- [2] B.L. Györfy *et al.*, in *Alloy Phase Stability*, edited by G. Stocks and A. Gonis (Kluwer Academic Publishers, Dordrecht, 1989), p. 421.
- [3] F. Ducastelle, in *Order and Phase Stability in Alloys*, edited by F. de Boer and D. Pettifor (North-Holland, Amsterdam, 1991).
- [4] J.D. Althoff, D.D. Johnson, and F.J. Pinski (to be published).
- [5] *Binary Alloy Phase Diagrams*, edited by B. Massalski, H. Okamoto, P.R. Subramanian, and L. Kacprzak (ASM International, New York, 1990), 2nd ed.
- [6] As compiled in H. Thomas, *Z. Metallk.* **63**, 106 (1977), and references therein.
- [7] L. Rheinhard *et al.*, *Phys. Rev. B* **41**, 1727 (1990).
- [8] G.J.L. Van Der Wegen *et al.*, *Scr. Metall.* **15**, 1359 (1981).
- [9] S. Hashimoto *et al.*, *J. Phys. Soc. Jpn.* **54**, 3796 (1985).
- [10] G. Ceder *et al.*, *Phys. Rev. B* **49**, 1 (1994).
- [11] A. De Rooy *et al.*, *Acta Metall.* **28**, 1339 (1980).
- [12] A. De Rooy *et al.*, *Scr. Metall.* **15**, 1362 (1981).
- [13] B. Moser, D.T. Keating, and S.C. Moss, *Phys. Rev. B* **175**, 868 (1968).
- [14] A. Khachaturyan, *Theory of Structural Transformations in Solids* (John Wiley and Sons, New York, 1983).
- [15] J.B. Staunton, D.D. Johnson, and F.J. Pinski, *Phys. Rev. B* **50**, 1450 (1994).
- [16] D.D. Johnson, J.B. Staunton, and F.J. Pinski, *Phys. Rev. B* **50**, 1473 (1994).
- [17] D. Badalyan, A. Khachaturyan, and A. Kitaigorodskii, *Sov. Phys. Crystallogr.* **14**, 333 (1969).
- [18] B.L. Györfy and G.M. Stocks, *Phys. Rev. Lett.* **50**, 374 (1983).
- [19] S.C. Moss, *Phys. Rev. Lett.* **22**, 1108 (1969).
- [20] Neil W. Ashcroft and N. David Mermin, *Solid State Physics* (Saunders College, Philadelphia, PA, 1976).